Earth and Planetary Science Letters 376 (2013) 99–109

Contents lists available at SciVerse ScienceDirect

Earth and Planetary Science Letters

www.elsevier.com/locate/epsl

Biogenic magnetite, detrital hematite, and relative paleointensity in Quaternary sediments from the Southwest Iberian Margin

J.E.T. Channell [a,*], D.A. Hodell [b], V. Margari [c], L.C. Skinner [b], P.C. Tzedakis [c], M.S. Kesler [d]

[a] Department of Geological Sciences, POB 112120, University of Florida, Gainesville, FL 32611, United States
[b] Godwin Laboratory for Palaeoclimate Research, Department of Earth Sciences, University of Cambridge, Cambridge CB2 3EQ, UK
[c] Department of Geography, University College London, Pearson Building, Gower Street, London WC1E 6BT, UK
[d] Major Analytical Instrumentation Center (MAIC), University of Florida, Gainesville, FL 32611, United States

ARTICLE INFO

Article history:
Received 16 September 2012
Received in revised form 10 June 2013
Accepted 12 June 2013
Available online 3 July 2013
Editor: Dr. J. Lynch-Stieglitz

Keywords:
magnetic properties
Iberian Margin
relative paleointensity
biogenic magnetite

ABSTRACT

Magnetic properties of late Quaternary sediments on the SW Iberian Margin are dominated by bacterial magnetite, observed by transmission electron microscopy (TEM), with contributions from detrital titanomagnetite and hematite. Reactive hematite, together with low organic matter concentrations and the lack of sulfate reduction, lead to dissimilatory iron reduction and availability of Fe(II) for abundant magnetotactic bacteria. Magnetite grain-size proxies (κ_{ARM}/κ and ARM/IRM) and S-ratios (sensitive to hematite) vary on stadial/interstadial timescales, contain orbital power, and mimic planktic $\delta^{18}O$. The detrital/biogenic magnetite ratio and hematite concentration are greater during stadials and glacial isotopic stages, reflecting increased detrital (magnetite) input during times of lowered sea level, coinciding with atmospheric conditions favoring hematitic dust supply. Magnetic susceptibility, on the other hand, has a very different response being sensitive to coarse detrital multidomain (MD) magnetite associated with ice-rafted debris (IRD). High susceptibility and/or magnetic grain-size coarsening, mark Heinrich stadials (HS), particularly HS2, HS3, HS4, HS5, HS6 and HS7, as well as older Heinrich-like detrital layers, indicating the sensitivity of this region to fluctuations in the position of the polar front. Relative paleointensity (RPI) records have well-constrained age models based on planktic $\delta^{18}O$ correlation to ice-core chronologies, however, they differ from reference records (e.g. PISO) particularly in the vicinity of glacial maxima, mainly due to inefficient normalization of RPI records in intervals of enhanced hematite input.

1. Introduction

A series of sediment cores retrieved from the SW Iberian Margin by the R/V *Marion Dufresne* in 1995, 1999 and 2001 contain important archives not only of North Atlantic climate (e.g., Martrat et al., 2007) but also continental climate through marine pollen records (Tzedakis et al., 2009; Margari et al., 2010). Evidence for linkages between northern and southern hemisphere climate have been documented in this region from planktic and benthic $\delta^{18}O$ that record Greenland and Antarctic signals, respectively (Shackleton et al., 2000, 2004), and confirm inter-hemispheric phasing of millennial-scale climate change during marine isotope stage (MIS) 3 inferred by methane synchronization of Greenland and Antarctic ice cores (Blunier and Brook, 2001; EPICA Community Members, 2006). Because of the northern (Greenland) and southern (Antarctic) influence on surface and deep water, respectively (see Skinner et al., 2003, 2007), the planktic $\delta^{18}O$ records from the SW Iberian Margin mimic stadial–interstadial oscillations from Greenland ice (Shackleton et al., 2000, 2004) whereas the benthic $\delta^{18}O$ signal resembles Antarctic temperature variations. Within MIS 3, Antarctic warm events occur during the longest, coldest stadials in Greenland, and are followed by abrupt warming in Greenland as Antarctica began to cool. This pattern has been referred to as the "bipolar seesaw" (e.g., Broecker, 1998) and is explained by changes in heat transport related to large-scale thermohaline circulation (Atlantic Meridional Overturning Circulation). In addition, the Iberian Margin cores exhibit concentrations of coarse (> 90 μm) lithic grains, marked by peaks in magnetic susceptibility, that are associated with ice-rafted debris (IRD) deposited during Heinrich stadials (HS)1, HS2, HS3, HS4, HS5 and HS6 (Thouveny et al., 2000; Moreno et al., 2002; Skinner et al., 2003; Vautravers and Shackleton, 2006; Voelker and de Abreu, 2011).

The *Marion Dufresne* (MD) cores collected in 1995 from the SW Iberian Margin (MD95-2039, -2040 and -2042) have been used to determine records of relative paleointensity (RPI) of the geomagnetic field, leading to the construction of a Portuguese Margin RPI stack (Thouveny et al., 2004). The RPI studies were carried out in conjunction with studies of $^{10}Be/^{9}Be$ in sediments from

* Corresponding author. Tel.: +352 392-3658; fax: +352 392 9294.
E-mail address: jetc@ufl.edu (J.E.T. Channell).

0012-821X/$ – see front matter
http://dx.doi.org/10.1016/j.epsl.2013.06.026

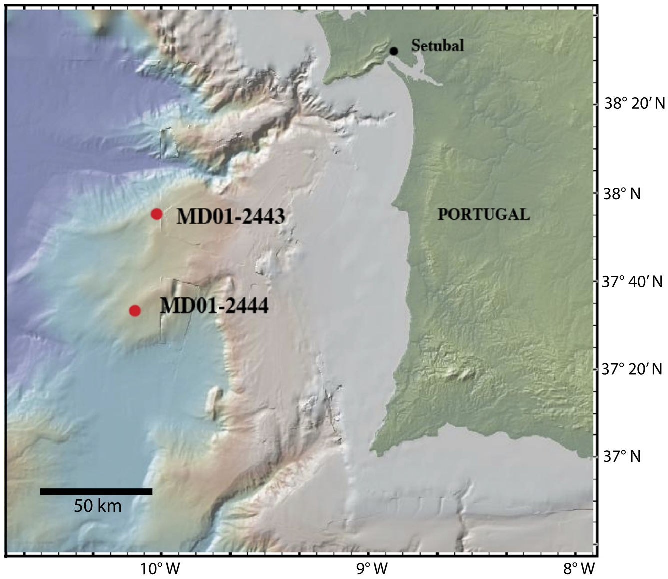

Fig. 1. Location of Cores MD01-2443 and MD01-2444 (from GeoMapApp™).

the same cores, which can be related to ^{10}Be flux in ice cores, atmospheric ^{10}Be production, and hence to RPI (Carcaillet et al., 2003, 2004a, 2004b; Ménabréaz et al., 2011). Magnetic parameters have indicated finer magnetite grain sizes during interglacials, when sortable-silt grain sizes imply stronger bottom current flow, and according to Moreno et al. (2002), magnetic grain-size parameters reflect varying detrital sources whereas physical sortable-silt grain size is controlled by local bottom-current strength.

Here we describe magnetic properties and RPI records from two MD piston cores collected in 2001 from the SW Iberian Margin (Fig. 1). Core MD01-2443 (37°52.85′N, 10°10.57′W, 2925 m water depth) and Core MD01-2444 (37°33.68′N, 10°8.53′W, 2637 m water depth) are 27 m and 29.5 m in length and extend into marine isotope stage (MIS) 11 and MIS 6, respectively.

The centennial timescales associated with non-axial dipole (NAD) components of the geomagnetic field (e.g., Lhuillier et al., 2011) implies that RPI, when measured in sediments with sedimentation rates less than a few decimeters/kyr, are largely devoid of NAD components are therefore useful for global correlation at millennial or multi-millennial timescales (see Channell et al., 2009). This study of cores from the SW Iberian Margin was prompted by the need for high-resolution RPI records to augment the existing reference template, by the availability of high-quality age control at this location through δ^{18}O (Shackleton et al., 2004), and by the apparent suitability of magnetic properties for RPI studies (Thouveny et al., 2004). In November 2011, Integrated Ocean Drilling Program (IODP) Expedition 339 occupied IODP Site U1385 (37°34.29′N, 10°7.56′W), located close to Core MD01-2444 (see Stow et al., 2012).

2. Age model

The close similarity of the planktic δ^{18}O records from the SW Iberian Margin and δ^{18}O of Greenland ice cores over the last glacial cycle (Shackleton et al., 2000, 2004; Skinner et al., 2003) allows Greenland age models to be adopted for SW Iberian Margin sediments. The age model for Core MD01-2444 for the last glacial cycle was constructed by correlation of the MD01-2444 planktic δ^{18}O record to the Greenland ice-core record, using the revised Greenland chronology of Shackleton et al. (2004). For Cores MD01-2443 and MD01-2444, beyond the last glacial cycle, we use an age model derived by correlating millennial variability in the δ^{18}O records to a synthetic Greenland δ^{18}O record produced using the EPICA Dome C (EDC) ice core and a thermal bipolar seesaw model (Barker et al., 2011; Hodell et al., 2013). The synthetic Greenland δ^{18}O record was placed on an absolute 'Speleo-Age' timescale by correlating cold events in the synthetic Greenland record with 'weak monsoon events' in the detrended speleothem record (Barker et al., 2011). Planktic δ^{18}O (Fig. 2b) and benthic δ^{18}O (Fig. 2c) data for MD01-2443 are available from marine isotope stage (MIS) 5 to the base of the section in MIS 11 (De Abreu et al., 2005; Tzedakis et al., 2004, 2009; Voelker and de Abreu, 2011). For Core MD01-2444 (0-200 ka), planktic oxygen isotope data (Fig. 2b) have been published in various studies (De Abreu et al., 2005; Vautravers and Shackleton, 2006; Skinner et al., 2007; Margari et al., 2010). For the last glacial cycle, back to 200 ka, the age model for Core MD01-2443 was constructed by correlation of the Ca/Ti ratio, determined by X-ray fluorescence (XRF) core scanning (Fig. 2d), between Cores MD01-2444 and MD01-2443 (see Hodell et al., 2013), and hence transfer of the Greenland chronology from Core MD01-2444 to MD01-2443. The resulting age models imply sedimentation rates in the 5–20 cm/kyr range and the 10–40 cm/kyr range for Cores MD01-2443 and MD01-2444, respectively (Fig. 2e).

3. Natural remanent magnetization (NRM)

Continuous u-channel samples ($2 \times 2 \times 150$ cm^3 samples encased in plastic with a clip-on lid constituting one of the sides) were collected from the archive halves of each 1.5 m section of Cores MD01-2443 and MD01-2444. Measurements of natural remanent magnetization (NRM) of u-channel samples were made at 1 cm intervals, with a 10 cm leader and trailer at the top and base of each u-channel sample, using a 2 G Enterprises pass-through magnetometer at the University of Florida designed for the measurement of u-channel samples (Weeks et al., 1993; Guyodo et al., 2002). After initial NRM measurement of u-channel samples, stepwise AF demagnetization was carried out in 5 mT increments in the 10–60 mT peak field interval, and in 10 mT increments in the 60–100 mT interval, using tracking speeds of 10 cm/s. Component magnetizations were computed each 1 cm for a uniform 20–80 mT demagnetization interval (see Supplementary Fig. S1) using the standard least-squares method (Kirschvink, 1980) without anchoring to the origin of the orthogonal projections, using UPmag software (Xuan and Channell, 2009). Supplementary materials related to this article can be found on-line at http://dx.doi.org/10.1016/j.epsl.2013.06.026. The maximum angular deviation (MAD) values are generally below 5° (see Supplementary Fig. S1), indicating well-defined magnetization components although the NRM is not fully demagnetized at peak fields of 100 mT, indicating that the NRM is partially carried by high-coercivity magnetic minerals. Component declinations (see Supplementary Fig. S1) were adjusted for vertical-axis core rotation by uniform rotation of the entire core such that the mean core declination is oriented North. Top-core twisting of sediment is apparent in the declination of Core MD01-2443 where the top 13 m of sediment (back to 110 ka) is affected (see Supplementary Fig. S1). For Core MD01-2444, the top 13 m (back to ∼ 50 ka) is also twisted although less so than core MD01-2443. Component inclinations are negative over about 10 cm of core at 13.5 ka (2.4 m depth) in Core MD01-2444 (see Supplementary Fig. S1), however, further investigations are required before these component directions can be attributed to the geomagnetic field. As has been often noted, the top ∼ 10–15 m of *Marion Dufresne* (MD) cores retrieved with the Calypso corer are usually "oversampled" (stretched) during recovery by ∼ 30–40% (see Széréméta et al., 2004), possibly account-

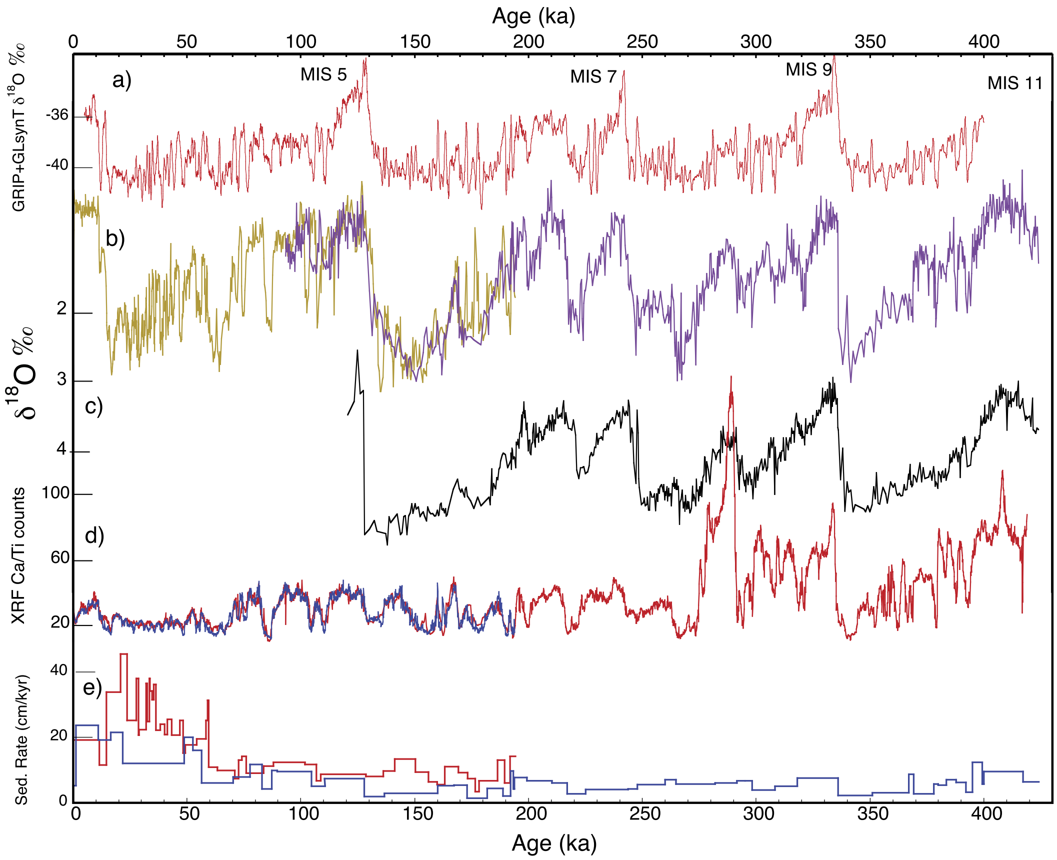

Fig. 2. (a) Synthetic Greenland ice-core $\delta^{18}O$ derived from Antarctic ice cores (see Barker et al., 2011). (b) Planktic $\delta^{18}O$ record for MD01-2444 (brown) and MD01-2443 (purple). (c) Benthic $\delta^{18}O$ record for MD01-2443 (black). (d) XRF scanning Ca/Ti counts for MD01-2444 (blue) and MD01-2443 (red) correlated to transfer the MD01-2444 age model to MD01-2443. (e) Sedimentation rates for MD01-2444 (red) and MD01-2443 (blue). (For interpretation of the references to color in this figure legend, the reader is referred to the web version of this article.)

ing for the anomalous features in magnetic parameters in the top 10–15 m.

4. Relative paleointensity (RPI)

The intensity of a detrital remanent magnetization (DRM) depends on the intensity of the geomagnetic field, and the concentration and alignment efficiency of remanence-carrying grains. In favorable circumstances, the relative strength of the magnetizing field can be determined by using the intensity of different types of laboratory-induced magnetizations, anhysteretic remanent magnetization (ARM) and isothermal remanent magnetization (IRM), to normalize the NRM intensity for changes in concentration of remanence-carrying grains. The normalizer should, therefore, activate the same grains that carry the NRM. The resulting normalized remanence can be a proxy for relative paleointensity (RPI) variations if magnetite is the sole NRM carrier and occurs in a restricted grain-size range (Banerjee and Mellema, 1974; Levi and Banerjee, 1976; King et al., 1983; Tauxe, 1993).

ARM was acquired in a peak alternating field of 100 mT and a DC bias field of 50 µT, then demagnetized at the same peak fields used to demagnetize the NRM. Subsequently, stepwise acquisition of ARM (ARMAQ) was carried out using a uniform bias field (50 µT) and increasing values of peak alternating field in the same steps as for stepwise demagnetization. $IRM_{0.3T}$ was acquired using impulse fields of 0.3 T, demagnetized in the same peak fields as applied to the NRM and ARM, and then an additional IRM_{1T}, acquired in impulse fields of 1T, was demagnetized once more in the same peak demagnetization fields. This RPI protocol (see Channell et al., 2002) allows us to calculate four RPI proxies as slopes: NRM/ARM, NRM/ARMAQ, NRM/$IRM_{0.3T}$, and NRM/IRM_{1T} all calculated for the 20–60 mT demagnetization or acquisition interval (Fig. 3a, b) using the UPmag software of Xuan and Channell (2009). Linear correlation coefficients (r) associated with each slope indicate that the slopes are generally well defined with r-values > 0.98. The RPI proxies for Core MD01-2443 and MD01-2444, when placed on their respective age models, can be matched to each other, to the Portuguese Margin RPI stack (Thouveny et al., 2004) and to the PISO RPI stack of Channell et al. (2009), although the correspondence is poor particularly in the vicinity of glacial maxima (shaded in Fig. 3c).

5. Rock magnetism

In addition to the data acquired in the process of NRM and RPI investigations, volume susceptibility (κ) was measured at 1-cm intervals using a susceptibility track designed for u-channel samples that has a Gaussian-shaped response function, with width at half height of ~ 4 cm, similar to the response function of the u-channel magnetometer (Thomas et al., 2003). Following King et al. (1983), the ratio of anhysteretic susceptibility (κ_{ARM}, ARM intensity divided by the DC bias field used to acquire the ARM) to susceptibility (κ) can be used to estimate grain size in magnetite. The values of this ratio for Cores MD01-2443 and MD01-2444 (Fig. 4a) show a wide range of magnetite grain size, and are unusual for North Atlantic pelagic sediments where magnetite grain sizes are usually centered around 5 µm for drift sediments, or ~ 1 µm for abyssal sites such as Site U1308 (e.g. Channell et al., 2008). Values below 1 µm in Cores MD01-2443 and MD01-2444 (Fig. 4a) imply that the magnetite is partially biogenic in origin, although

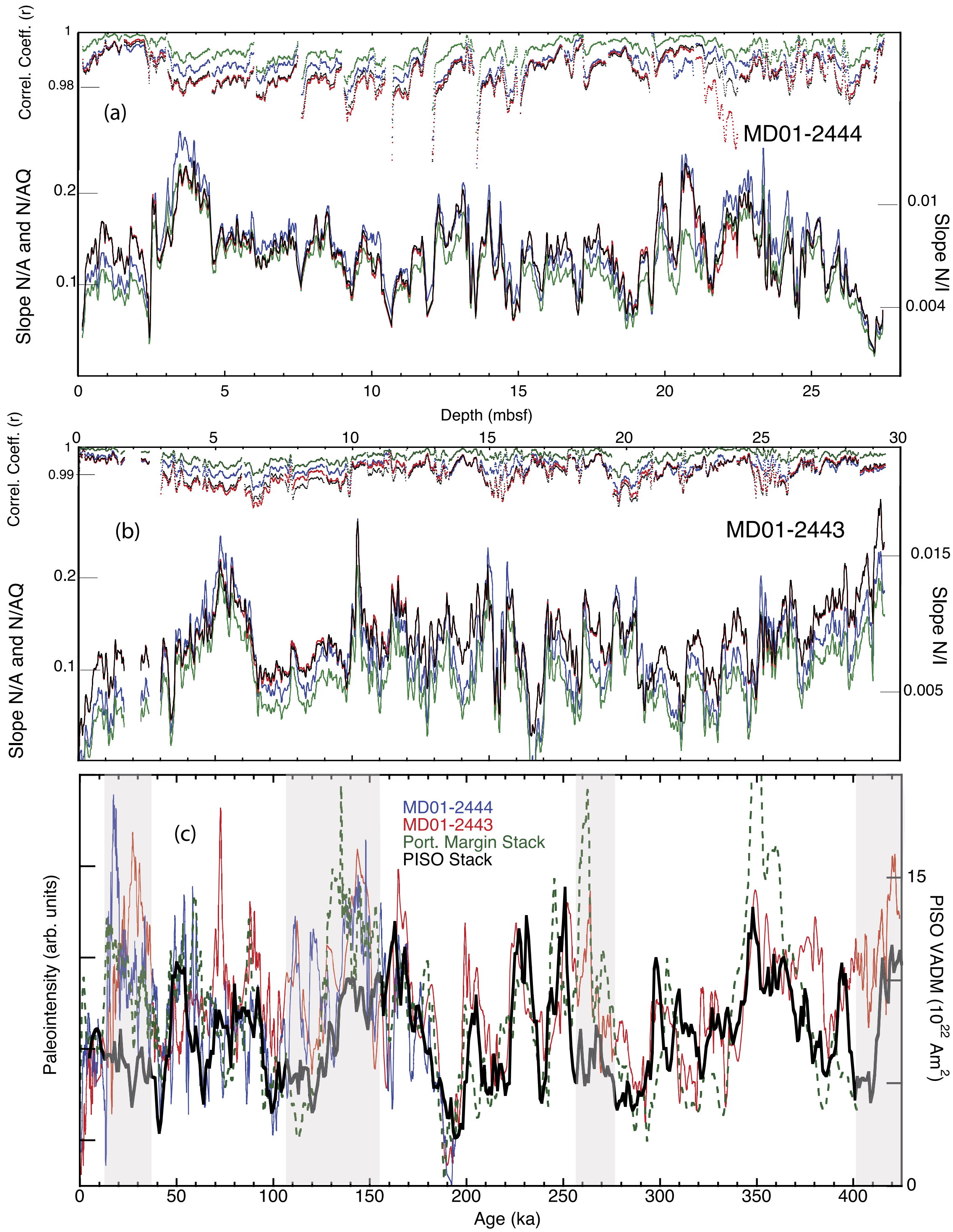

Fig. 3. MD01-2444 (a) and MD01-2443 (b) relative paleointensity (RPI) proxies: Slopes of NRM/ARM (blue), NRM/ARMAQ (green), NRM/IRM_{1T} (red) and NRM/$IRM_{0.3T}$ (black) and corresponding linear correlation coefficients (r) with the same color code. Slopes were all calculated for the 20–60 mT peak field demagnetization interval. (c) Relative paleointensity proxies for MD01-2444 (blue) and MD01-2443 (red) on the age models derived through Fig. 2, compared with the Portuguese Margin stack (dashed, green) (Thouveny et al., 2004) and the PISO paleointensity stack (black) (Channell et al., 2009). Major discrepancies in the fit of RPI proxies for Cores MD01-2444 and MD01-2443 to the PISO stack are shaded. (For interpretation of the references to color in this figure legend, the reader is referred to the web version of this article.)

the spread of grain size implies other (detrital) inputs. One of the characteristics of biogenic (bacterial) magnetite is grain size constrained to < 100–200 nm, markedly smaller than the range of grain sizes associated with detrital magnetite in pelagic deep-sea sediments.

Variations in magnetite grain-size proxies (κ_{ARM}/κ and ARM/IRM) mimic planktic $\delta^{18}O$ in Core MD01-2444 (Fig. 5) and MD01-2443 (Fig. 6), indicating finer/coarser magnetite grain sizes during interstadials/stadials. The measurement of $IRM_{0.3T}$ and IRM_{1T} (see above) allows us to calculate a "forward S-ratio" (see Heslop, 2009) calculated as the ratio: $IRM_{0.3T}/IRM_{1T}$. The S-ratio mimics both the magnetite grain-size proxies (κ_{ARM}/κ and ARM/IRM) and planktic $\delta^{18}O$ at stadial/interstadial scales (Figs. 5 and 6). The S-ratio is sensitive to the concentration of high-

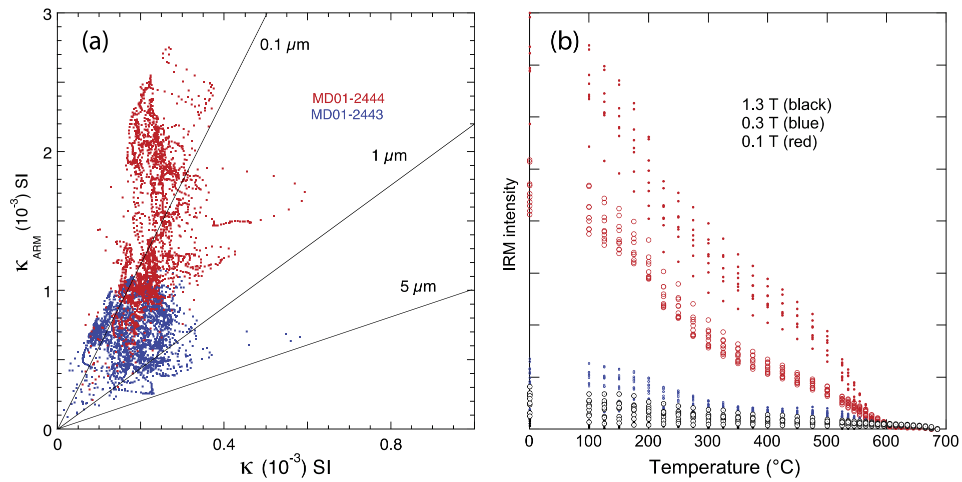

Fig. 4. (a) Plot of anhysteretic susceptibility (κ_{ARM}) against susceptibility (κ) for MD01-2444 (red in the web version) and MD01-2443 (blue in the web version) with the calibration of magnetite grain size from King et al. (1983). (b) Thermal demagnetization of a 3-axis isothermal remanence (IRM) from Core MD01-2444 acquired orthogonally and sequentially in DC fields of 1.3 T, 0.3 T and 0.1 T. Closed and open symbols represent samples from interglacial (MIS 5) and glacial (MIS 6) stages, respectively.

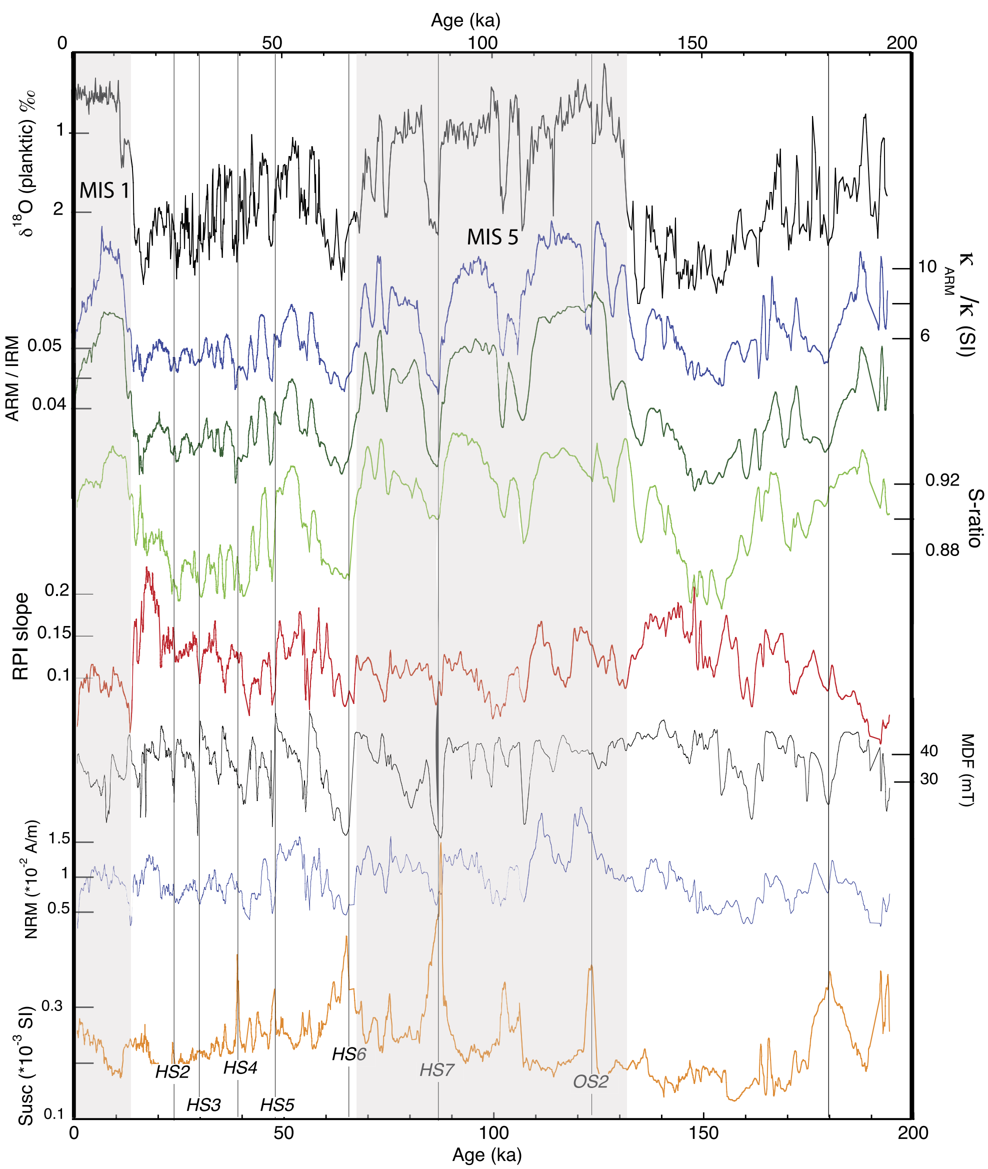

Fig. 5. Core MD01-2444: Comparison of planktic $\delta^{18}O$ with rock magnetic parameters sensitive to magnetite grain size (κ_{ARM}/κ, ARM/IRM), S-ratio (hematite proxy), relative paleointensity (RPI) proxy, median destructive field (MDF) of natural remanent magnetization (NRM) intensity, NRM intensity, and volume susceptibility. Vertical lines mark Heinrich stadials (HS). Marine isotope stages (MIS 1 and MIS 5) are labeled and shaded.

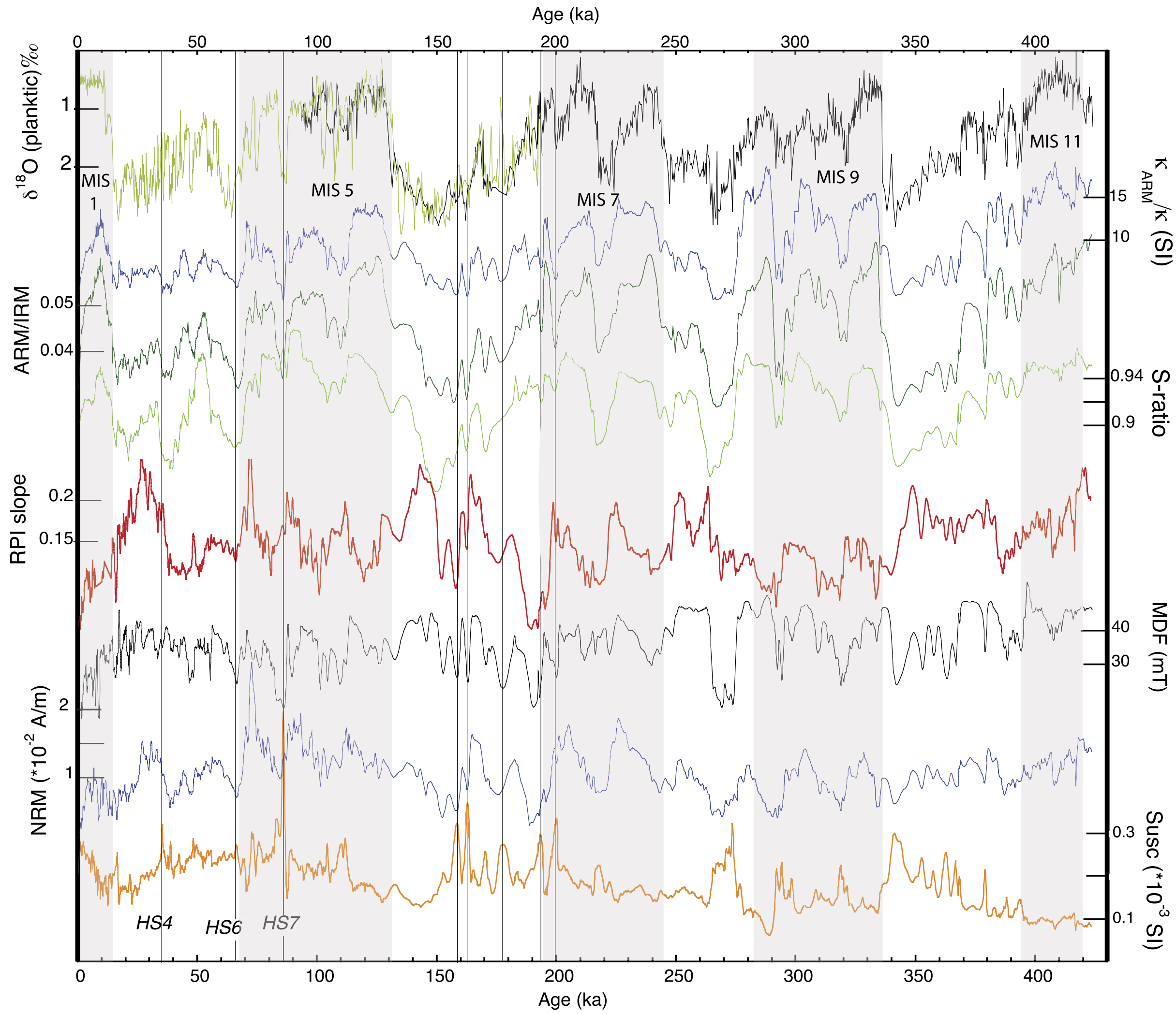

Fig. 6. Core MD01-2443: Comparison of planktic δ^{18}O (black, with record transferred from Core MD01-2444 in green) with rock magnetic parameters sensitive to magnetite grain size (κ_{ARM}/κ, ARM/IRM), S-ratio (hematite proxy), the relative paleointensity (RPI) proxy, median destructive field (MDF) of natural remanent magnetization (NRM), NRM intensity, and volume susceptibility. Vertical lines mark Heinrich stadials (HS) and Heinrich-like susceptibility features in MIS 6. Interglacial marine isotope stages (MIS) are labeled and shaded. (For interpretation of the references to color in this figure legend, the reader is referred to the web version of this article.)

coercivity minerals such as hematite and is not influenced by magnetite concentration or grain size. S-ratio values reach minima of ~ 0.85 during stadials/glacials (Figs. 4 and 5) implying enhanced hematite content at these times, coincident with enhanced input of coarser magnetite. Magnetite grain-size proxies and S-ratio exhibit power at orbital periods, with high coherency one to another, and with δ^{18}O (Supplementary Fig. S2). The median destructive field (MDF) of NRM tends to show low values when susceptibility is high, at times of magnetite grain-size coarsening, although values of MDF often exceed 40 mT implying that hematite contributes to the NRM (Figs. 5 and 6).

The thermal unblocking of a composite isothermal remanence (IRM) imposed sequentially and orthogonally in DC fields of 1.3 T, 0.3 T and 0.1 T for 18 samples from marine isotope stage (MIS) 5 and MIS 6 in Core MD01-2444 indicates that the IRM of these samples is dominated by low-coercivity magnetite with maximum blocking temperature of 580 °C, but with a discernable high-coercivity (hematite) signal that unblocks in the 580–680 °C interval particularly in samples taken from glacial MIS 6 (Fig. 4b).

Susceptibility peaks in Cores MD01-2444 and MD01-2443 (Figs. 5 and 6) can be matched to lithic counts in the same cores (Skinner et al., 2003; Vautravers and Shackleton, 2006), and to susceptibility peaks in nearby Core MD95-2042 (Thouveny et al., 2000; Moreno et al., 2002). Peaks in magnetic susceptibility, coarsening in magnetic grain-size proxies (κ_{ARM}/κ and ARM/IRM), low values of S-ratio (high hematite content), and lows in the MDF of NRM (Figs. 5 and 6) correspond to the following Heinrich stadials (HS): HS2, HS4. HS5, HS6 and HS7 (at ~ 87 ka). Correlative susceptibility peaks have been documented in Core MD95-2042 and in other MD cores from the Gulf of Cadiz (Moreno et al., 2002; Llave et al., 2006) and in cores from the central Atlantic, NE of the Azores (Robinson, 1986). “OS2” in Fig. 5 is a high susceptibility coarse-magnetite feature in MIS 5 (~ 123 ka) that may correlate with an “outburst flood event” of Laurentide origin recognized at Orphan Knoll (Labrador Sea) and on the Eirik Drift (Nicholl et al., 2012). Further back in time (Fig. 6), high susceptibility features denoting coarse-grained magnetite (low κ_{ARM}/κ and ARM) appear to correspond to susceptibility peaks recorded in Core MD95-2040, particularly those labeled S10–S15 in MIS 6–7 by Moreno et al. (2002).

Additional mineralogical information was acquired using magnetic hysteresis data measured on a Princeton Measurements Corp. vibrating sample magnetometer (VSM). Hysteresis ratios: M_r/M_s and H_{cr}/H_c where M_r is saturation remanence, M_s is saturation magnetization, H_{cr} is coercivity of remanence, and H_c is coercive force, can be used to delineate single domain (SD), pseudo-

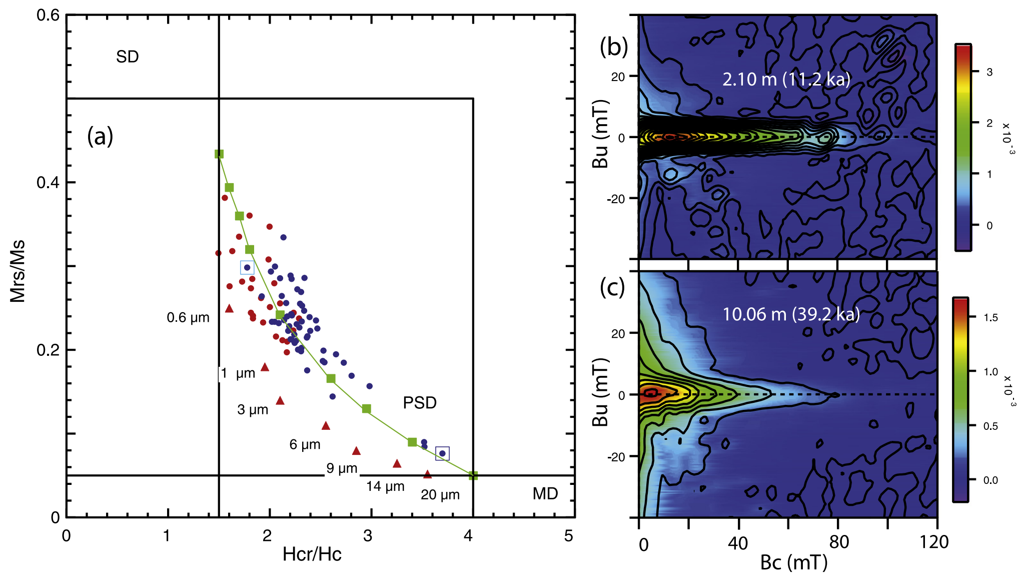

Fig. 7. (a) Hysteresis ratio plot after Day et al. (1977) for samples from Core MD01-2444 (blue circles) and Core MD01-2443 (red circles) lying along a magnetite grain-size mixing line (green squares and line, see text) in the pseudo-single domain (PSD) field, between the single domain (SD) and multidomain (MD) fields. Red triangles: hysteresis ratios from crushed, sized (unannealed) natural titanomagnetite (Dunlop, 2002). (b) First-order reversal curve (FORC) from Core MD01-2444, typical for samples from Cores MD01-2443 and MD01-2444 (implying biogenic magnetite). (c) FORC for sample from Heinrich stadial H4 in Core MD01-2444. Hysteresis ratios corresponding to FORC diagrams ((b) and (c)) are marked by blue squares in (a), and lie at the fine-grained and coarse-grained ends of the SD-MD mixing line, respectively. FORC diagrams constructed using smoothing factor = 6. (For interpretation of the references to color in this figure legend, the reader is referred to the web version of this article.)

single domain (PSD) and multidomain (MD) magnetite and to assign "mean" magnetite grain sizes through empirical and theoretical calibrations of the so-called Day plot (Day et al., 1977; Carter-Stiglitz et al., 2001; Dunlop, 2002; Dunlop and Carter-Stiglitz, 2006). Magnetic hysteresis properties were also analyzed through First-Order Reversal Curves (FORCs) that provide enhanced mineral and domain state discrimination (Pike et al., 1999; Roberts et al., 2000; Muxworthy and Roberts, 2007). FORCs are carried out by progressively saturating a small (few hundred mg) sample in a field (H_{sat}), decreasing the field to a value H_a, reversing the field and sweeping it back to H_{sat} in a series of regular field steps (H_b). The process is repeated for many values of H_a. The magnetization is then represented as a contour plot with axes B_c and B_u where $B_c = (H_b - H_a)/2$ and $B_u = (H_b + H_a)/2$. The contoured distribution of a FORC can be interpreted in terms of the coercivity distribution along the B_c axis. Spreading of the distribution along the B_u axis corresponds to magnetostatic interactions for SD grains or internal demagnetizing fields for MD grains, although the latter dominates in weakly magnetized deep-sea sediments, and spreading in B_u combined with low B_c can be interpreted in terms of high MD magnetite content. In general, closed peaked structures along the B_c axis are characteristic of SD gains, with contours becoming progressively more parallel to the B_u axis with grain-size coarsening. FORC diagrams were analyzed using the software of Harrison and Feinberg (2008) with smoothing factors (SF) of 6 for a protocol using an averaging time of 1 s and a field increment of 2 mT up to a maximum applied field of 1 T.

Hysteresis ratios for Cores MD01-2444 and MD01-2443 placed on the Day plot usually lie in the submicron part of the magnetite-mixing curve (Fig. 7a), with no indication for the presence of hematite that can be explained by the dominating role of magnetite and by maximum applied field (1T) being insufficient to activate fine grained hematite. FORC diagrams are usually characterized by a pronounced ridge (Fig. 7b) aligned along the B_c axis, and very weak particle interaction (B_u), implying dispersed fine-grained magnetite of probable biogenic origin (see examples in Egli et al., 2010; Roberts et al., 2011, 2012; Yamazaki, 2012). FORC diagrams with a pronounced ridge (Fig. 7b) were found to be typical of glacial and interglacial stages of Cores MD01-2444 and MD01-2443. In contrast, FORC diagrams from Heinrich layers (e.g. HS4) show low coercivities (B_c) and higher degree of particle interaction (B_u) implying MD magnetite within IRD (Fig. 7c). Hysteresis ratios associated with H4 indicate magnetite grain sizes of several tens of microns, approaching the MD field in the Day et al. (1977) hysteresis diagram (Fig. 7a).

6. Transmission electron microscopy

For transmission electron microscopy (TEM), three magnetic extracts were prepared from Core MD01-2444 (Early Holocene sample), and Core MD01-2443 (MIS 8 and MIS 9 samples) by sonicating ~ 20 cm^3 of sediment in a sodium metaphosphate dispersant. The solution was loaded into a reservoir feeding a circulating system driven by a peristaltic pump that allowed the fluid to pass slowly, without turbulence, past the outside of a test-tube containing a rare-earth magnet. The material that adhered to the outside of the test-tube was then removed to a methanol solution using a methanol squeeze-bottle. Grains of magnetic separate were encouraged to adhere to a 3 mm Type-B copper TEM grid using another magnet suspended a few cm above the floating grid. This "wet" extraction procedure does not allow good estimates of the efficiency of extraction, and the extraction procedure is undoubtedly selective and may favor biogenic magnetite (see Wang et al., 2013).

Observations were made using a JEOL JEM-2010F high-resolution (HR) TEM in conjunction with energy dispersive x-ray spectroscopy (EDS) at an accelerating voltage of 200 kV. The microscope is equipped with a Gatan MultiScan Camera Model 794 for imaging and an Oxford Instruments detector with INCA 4.05 software for microanalysis. Spot analysis and line-scans were conducted in STEM mode with a nominally ~ 1 nm probe size and a camera length of 12 cm.

Euhedral grains, generally smaller than 100 nm across, but occasionally reaching 200 nm, were observed in all three magnetic extracts (Fig. 8), with shape and size consistent with these grains (magnetosomes) having been produced by magnetotactic bacteria (see Kopp and Kirschvink, 2008; Egli et al., 2010; Roberts et al., 2011, 2012; Yamazaki, 2012). No clear differences in magne-

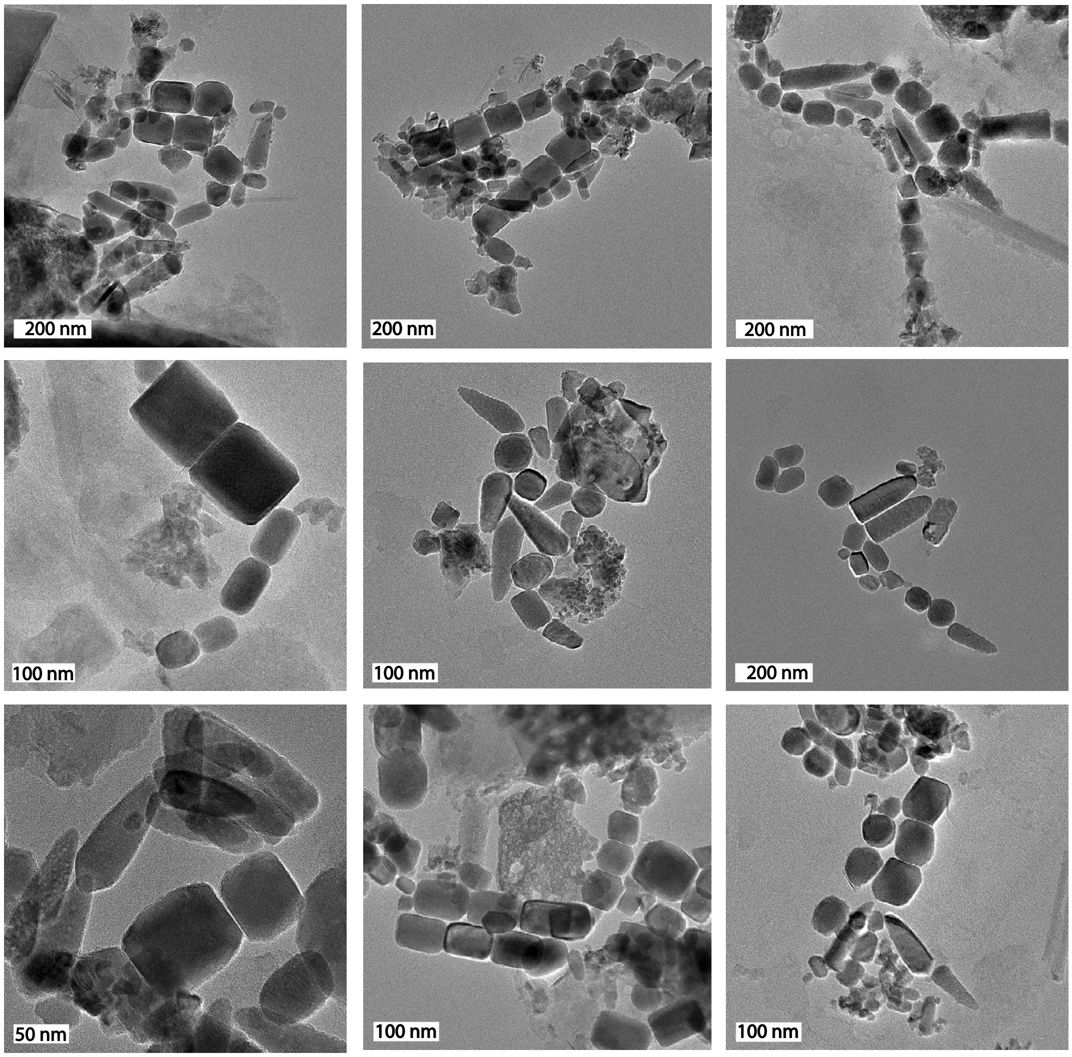

Fig. 8. Transmission electron microscope (TEM) images of magnetic extracts. Top row: Core MD01-2444 (early Holocene). Middle row: Core MD01-2443 (MIS 8). Bottom row: Core MD01-2443 (MIS 9). Particle size and shape (including octagons, arrowheads and bullets) are consistent with biogenic magnetite. White bar gives scale.

tosome population were observed for Early Holocene, MIS 8 or MIS 9 (Fig. 8) with magnetite octagons (rectangular shapes with flattened corners), arrowheads and bullet-shapes occurring in all three extracts. Detrital magnetite was also observed, particularly in the extract from MIS 8 (Fig. 9), appearing as larger (several μm-scale) grains of irregular shape. EDS elemental analyses indicate that the detrital grains contain Fe, O and Ti, whereas the finer euhedral (biogenic) magnetites contain Fe and O, but no detectable Ti (Fig. 9), thereby providing a means, other than size and shape, of distinguishing magnetite of detrital and biogenic origin.

In Fig. 10, the size and shape of 518 euhedral (biogenic) magnetite grains, determined from TEM images using *ImageJ64* software, are compared with the theoretical fields for interacting and non-interacting SD and MD grains, and modern examples of interacting and non-interacting magnetosome populations from Hungary (Muxworthy and Williams, 2006; Arato et al., 2005). We see that the distribution of grain lengths and axial ratios are not distinguishable for the three extracts (Early Holocene, MIS 8 and MIS 9). The measured grains lie in the non-interacting SD field for width/length ratios $<\sim 0.6$, and encroach into the interacting fields for ratios $>\sim 0.6$ (Fig. 10). This implies that grains with lower width/length ratios ($<\sim 0.6$), such as the bullet and arrowhead shapes (Fig. 8), existed as isolated SD grains within bacteria. Grains with higher width/length ratios ($>\sim 0.6$) lie in the interacting field of Fig. 10, and occasionally occur as partially intact magnetosome chains in TEM micrographs (Fig. 8), implying these grains were part of interacting chains. Up/down navigation is usually assumed to be the role of bacterial magnetosomes, allowing motility to optimal redox conditions in surface sediment (e.g. Kopp and Kirschvink, 2008).

7. Discussion and conclusions

Linear correlation coefficients associated with RPI proxies (slopes) are generally > 0.98 indicating well-defined RPI proxies for Cores MD01-2443 and MD01-2444 (Fig. 3a, b). RPI proxies can be matched between the two sites and to the lower-resolution PISO stack, although there are obvious discrepancies, particularly within or close to glacial maxima and glacial terminations (Fig. 3c) where low values of the S-ratio (Figs. 5 and 6) indicate enhanced hematite content. The presence of hematite is also indicated by thermal demagnetization of IRM (Fig. 4b), and by reflectance data (see Hodell et al., 2013). The normalization procedures that result in RPI proxies are not designed for NRMs carried, even partially, by hematite. On the other hand, comparison of the NRM/IRM$_{0.3T}$ and NRM/IRM$_{1T}$ RPI proxies would be expected to be sensitive to variations in S-ratio, and yet these two RPI proxies are broadly consistent with one another (Fig. 3a, b). At both sites, the median

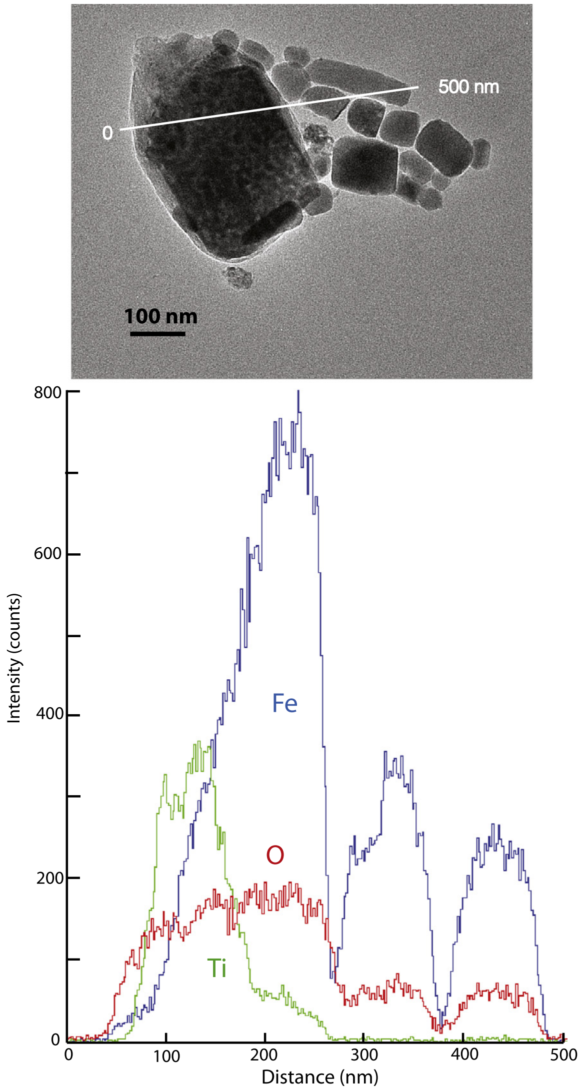

Fig. 9. TEM micrograph of a detrital magnetite grain, and a group of smaller biogenic magnetite grains, overlain by a line indicating the position of a 500 nm long energy dispersive X-ray spectroscopy (EDS) line-scan, with plot of intensity (Fe, O and Ti) versus distance along that line. Note that gaps between grains are observed in the intensity scan, and that the detrital magnetite grain contains Ti but the smaller biogenic magnetite grains do not.

destructive fields (MDFs) of NRM determined from AF demagnetization often exceed 40 mT (Figs. 5 and 6), and exhibit low values when S-ratios are low (high hematite content) and when magnetite grain-size proxies indicate coarsening. These observations imply that detrital (coarser) low-coercivity magnetite during stadials/glacials reduces MDF, and dominates over the effect of higher hematite content.

Variations in carbonate concentrations in sediments from this region, as monitored by the Ca/Ti from XRF scans (Fig. 2), have been associated with changes in terrigenous supply associated with sea-level, rather than changes in surface water productivity and dilution by biogenic carbonate (Thomson et al., 1999, 2000). Magnetite grain-size proxies vary not only with $\delta^{18}O$ (Figs. 5 and 6) but also with Ca/Ti (Fig. 2d) indicating coarse (detrital) magnetite during glacials/stadials at times of enhanced detrital input denoted by low values of Ca/Ti. Hodell et al. (2013) have shown, in these same cores, that a* (red-brown) reflectance and the change in reflectance in the 570–560 nm waveband (diagnostic of hematite abundance) are coherent and in-phase with S-ratio, particularly at periods corresponding to orbital precession. These

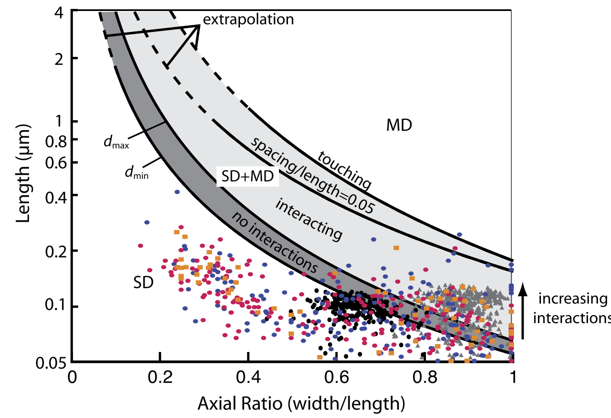

Fig. 10. Size and shape of biogenic magnetite from Core MD01-2443 marine isotope stage (MIS) 8 (blue circles), MIS 9 (red circles) and Core MD01-2444 early Holocene (orange squares), measured from TEM images, superimposed on the theoretical curves of Muxworthy and Williams (2006) together with two modern populations (black and gray, respectively) of non-interacting freshwater magnetosomes from Malmo to Hungary and interacting magnetosome chains from Séd (Hungary) (see Arato et al., 2005; Muxworthy and Williams, 2006). (For interpretation of the references to color in this figure legend, the reader is referred to the web version of this article.)

authors have also shown that the detrital indicator (Ca/Ti) lags the hematite indicators by ~ 7 kyr. This can be explained by an atmospheric (dust) source for detrital hematite and a lagged response (sea-level forcing) for Ca/Ti and, hence, for detrital magnetite. In this scenario, the biogenic magnetite production on the seafloor is relatively constant, and ARM/IRM or κ_{ARM}/κ grain-size parameters are controlled by detrital magnetite input related to sea level. In nearby Core MD95-2040, fining of magnetite (from κ_{ARM}/κ) during interglacials/interstadials is accompanied by *increase* in the silt/clay ratio and coarsening of the sortable silt mean grain size (Moreno et al., 2002), indicating decoupling of magnetic and sortable-silt grain-size parameters. Whereas the sortable-silt parameter in Core MD95-2040 can be interpreted in terms of increased bottom-current strength during interglacials (Hall and McCave, 2000; Moreno et al., 2002), the κ_{ARM}/κ parameter is sensitive to submicron/micron scale magnetite that is well below the sortable-silt (10–63 μm) grain-size range. We interpret the stadial/interstadial variations in κ_{ARM}/κ (in MD95-2040 as well as in the cores studied here) in terms of the increased proportion of detrital versus biogenic magnetite, controlled by sea level, and not due to fluctuating deep-current transport of a fine detrital fraction from remote sources as suggested by Moreno et al. (2002).

The hysteresis ratio plot indicates that the magnetite grain sizes are largely submicron in size (Fig. 7a), based on comparison with the sized natural magnetite data of Dunlop (2002). The submicron grain size of magnetite is supported by high ARM intensity versus susceptibility values (Fig. 4a), implying an important contribution from biogenic (bacterial) magnetite. FORC diagrams indicate the presence of a well-defined narrow ridge elongated along the B_c axis (Fig. 7b) that is diagnostic of bacterial magnetite (Egli et al., 2010; Roberts et al., 2011, 2012; Yamazaki, 2012). The case for bacterial magnetite is supported by TEM observations of magnetite with size and shape similar to magnetosomes produced by modern magnetotactic bacteria (Fig. 8). EDS elemental analysis indicates that the fine-grained euhedral biogenic magnetite is devoid of detectable titanium whereas the detrital grains are typical titanomagnetites (Fig. 9). From TEM images, grain lengths and axial ratios for biogenic magnetite grains lie in the SD field for grains with lower axial ratios, and in the interacting field for grains with high width/length ratios (Fig. 10). This observation implies that grains with higher width/length ratios were part of magnetosome chains, some of which have remained partially intact in the magnetic extracts (Fig. 8).

Although bacterial magnetite is commonly encountered in dredges of modern sediment from marine and freshwater environments (e.g. Vali et al., 1987; Kopp and Kirschvink, 2008; Arato et al., 2005), biogenic magnetite is not always preserved in marine sediments due to the high surface-area to volume ratio of ultrafine grains that enhances reactivity, resulting in the formation of iron sulfides through reaction with sulfide ions produced by diagenetic sulfate reduction. The production and preservation of bacterial magnetite is therefore a balance between sufficient organic carbon and reactive iron to stimulate growth of magnetotactic bacteria, but insufficient organic carbon for reducing diagenetic conditions, sulfate reduction, and magnetite dissolution. On the NW Iberian continental shelf, $\sim$400 km to the north of the cores discussed here, high organic carbon contents related to upwelling result in diagenetic reduction of primary magnetite (Mohamed et al., 2010). On the other hand, at IODP Site U1385 (close to Core MD01-2444), pore-water sulfate concentrations have seawater values in the upper 40 m of the sediment sequence (Stow et al., 2012). Organic carbon content is low in the upper sediments at IODP Site U1385 ($<$ 1 wt%) implying that low organic carbon content explains the lack of microbial sulfate reduction (and magnetite dissolution) in the uppermost 50 mbsf, and hence the preservation of ultra-fine-grained bacterial magnetite in Cores MD01-2444 (and MD01-2443). Low organic carbon and hence the lack of pore-water sulfate reduction (e.g., Westrich and Berner, 1984; Froelich et al., 1979), as well as the presence of reactive fine-grained (possibly eolian) hematite favors activity of dissimilatory iron reducing bacteria (e.g. *Geobachter* and *Shewanella*) that generate Fe (II) that diffuses upward in the absence of free sulfide to the near-surface sediment for utilization by magnetotactic bacteria. The presence of fine-grained hematite and low organic carbon content of the sediments, therefore, can explain the unusually high abundance of bacterial magnetite in these sediments relative to elsewhere in the North Atlantic realm.

Acknowledgements

Research supported by US National Science Foundation grants OCE-0850413 and EAR-1014506 (to J.C.). We thank K. Huang for laboratory assistance, S. Crowhurst for help with core sampling, and A. Muxworthy for supplying the template for Fig. 10. We appreciate the editorial comments of Jean Lynch-Stieglitz and Dennis Kent. Data are available at http://doi.pangaea.de/10.1594/PANGAEA.811826.

Appendix A. Supplementary material

Supplementary material related to this article can be found online at http://dx.doi.org/10.1016/j.epsl.2013.06.026.

References

Arato, B., Szanyi, Z., Flies, C., Schüler, D., Frankel, R.B., Buseck, P.R., Posfai, M., 2005. Crystal-size and shape distributions of magnetite from uncultured magnetotactic bacteria as a potential biomarker. Am. Mineral. 90, 1233–1241.

Banerjee, S.K., Mellema, J.P., 1974. A new method for the determination of paleointensity from the ARM properties of rocks. Earth Planet. Sci. Lett. 23, 177–184.

Barker, S., Knorr, G., Edwards, R.L., Rarrenin, F., Putnam, A.E., Skinner, L.C., Wolff, E., Ziegler, M., 2011. 800,000 years of abrupt climate variability. Science 334, 347–351.

Blunier, T., Brook, E.J., 2001. Timing of millennial scale climate change in Antarctica and Greenland during the last glacial period. Science 291, 109–112.

Broecker, W.S., 1998. Paleocean circulation during the last deglaciation: A bipolar seesaw? Paleoceanography 13, 119–121.

Carcaillet, J.T., Bourles, D.L., Thouveny, N., 2004a. Geomagnetic dipole moment and ^{10}Be production rate intercalibration from authigenic ^{10}Be/^{9}Be for the last 1.3 Ma. Geochem. Geophys. Geosyst. 5 (5), Q05006, http://dx.doi.org/10.1029/2003GC000641.

Carcaillet, J.T., Bourles, D.L., Thouveny, N., Arnold, M., 2004b. A high resolution authigenic ^{10}Be/^{9}Be record of geomagnetic moment variations over the last 300 ka from sedimentary cores of the Portuguese Margin. Earth Planet. Sci. Lett. 219, 397–412.

Carcaillet, J.T., Thouveny, N., Bourles, D.L., 2003. Geomagnetic moment instability between 0.6 and 1.3 Ma from cosmonuclide evidence. Geophys. Res. Lett. 30 (15), 1792, http://dx.doi.org/10.1029/2003GL017550.

Carter-Stiglitz, B., Moskowitz, B., Jackson, M., 2001. Unmixing magnetic assemblages and the magnetic behavior of bimodal mixtures. J. Geophys. Res. 106 (B11), 26,397–26,411.

Channell, J.E.T., Hodell, D.A., Xuan, C., Mazaud, A., Stoner, J.S., 2008. Age calibrated relative paleointensity for the last 1.5 Myr at IODP Site U1308 (North Atlantic). Earth Planet. Sci. Lett. 274, 59–71.

Channell, J.E.T., Mazaud, A., Sullivan, P., Turner, S., Raymo, M.E., 2002. Geomagnetic excursions and paleointensities in the Matuyama Chron at Ocean Drilling Program Sites 983 and 984 (Iceland Basin). J. Geophys. Res. 107, 2114, http://dx.doi.org/10.1029/2001JB000491.

Channell, J.E.T., Xuan, C., Hodell, D.A., 2009. Stacking paleointensity and oxygen isotope data for the last 1.5 Myrs (PISO-1500). Earth Planet. Sci. Lett. 283, 14–23.

Day, R., Fuller, M., Schmidt, V.A., 1977. Hysteresis properties of titanomagnetites: Grain-size and compositional dependence. Phys. Earth Planet. Inter. 13, 260–267.

De Abreu, L., Abrantes, F.F., Shackleton, N.J., Tzedakis, P.C., McManus, J.F., Oppo, D.W., 2005. Ocean climate variability in the eastern North Atlantic during interglacial marine isotope stage 11: A partial analogue to the Holocene? Paleoceanography 20, PA3009, http://dx.doi.org/10.1029/2004/PA001091.

Dunlop, D.J., 2002. Theory and application of the Day plot (M_{rs}/M_s versus H_{cr}/H_c) 1. Theoretical curves and tests using titanomagnetite data. J. Geophys. Res. 107 (B3), 2056, http://dx.doi.org/10.1029/2001JB000486.

Dunlop, D.J., Carter-Stiglitz, B., 2006. Day plots of mixtures of superparamagnetic, single domain, pseudosingle domain, and multidomain magnetites. J. Geophys. Res. 111, B12S09, http://dx.doi.org/10.1029/2006JB004499.

Egli, R., Chen, A.P., Winklhofer, M., Kodama, K.P., Horng, C.-S., 2010. Detection of non-interacting single domain particles using first-order reversal curve diagrams. Geochem. Geophys. Geosyst. 11, Q01Z11, http://dx.doi.org/10.1029/2009GC002916.

EPICA Community Members, 2006. One-to-one coupling of glacial climate variability in Greenland and Antarctica. Nature 444, 796–798.

Froelich, P.N., Klinkhammer, G.P., Bender, M.L., Luedtke, N.A., Heath, G.R., Cullen, D., Dauphin, P., Hammond, D., Hartman, B., Maynard, V., 1979. Early oxidation of organic matter in pelagic sediments of the eastern equatorial Atlantic: Suboxic diagenesis. Geochim. Cosmochim. Acta 43, 1075–1090.

Guyodo, Y., Channell, J.E.T., Thomas, R., 2002. Deconvolution of u-channel paleomagnetic data near geomagnetic reversals and short events. Geophys. Res. Lett. 29, 1845, http://dx.doi.org/10.1029/2002GL014963.

Hall, I.R., McCave, I.N., 2000. Palaeocurrent reconstruction, sediment and thorium focusing on the Iberian Margin over the last 140 ka. Earth Planet. Sci. Lett. 178, 151–164.

Harrison, R.J., Feinberg, J.M., 2008. FORCinel: An improved algorithm for calculating first-order reversal curve distributions using locally weighted regression smoothing. Geochem. Geophys. Geosyst. 9, Q05016, http://dx.doi.org/10.1029/2008GC001987.

Heslop, D., 2009. On the statistical analysis of the rock magnetic S-ratio. Geophys. J. Int. 178, 159–161.

Hodell, D.A., Crowhurst, S., Skinner, L., Tzedakis, P.C., Margari, V., Channell, J.E.T., Kamenov, G., Maclachlan, S., Rothwell, G., 2013. Response of Iberian Margin sediments to orbital and suborbital forcing over the past 420 ka. Paleoceanography 28, 185–199, http://dx.doi.org/10.1002/paleo.20017.

Howell, P., Pisias, N., Ballance, J., Baughman, J., Ochs, L., 2006. ARAND Time-Series Analysis Software. Brown University, Providence RI.

King, J.W., Banerjee, S.K., Marvin, J., 1983. A new rock-magnetic approach to selecting sediments for geomagnetic paleointensity studies: Application to paleointensity for the last 4000 years. J. Geophys. Res. 88, 5911–5921.

Kirschvink, J.L., 1980. The least squares lines and plane analysis of paleomagnetic data. Geophys. J. R. Astron. Soc. 62, 699–718.

Kopp, R.E., Kirschvink, J.L., 2008. The identification and biogeochemical interpretation of fossil magnetotactic bacteria. Earth-Sci. Rev. 86, 42–61.

Levi, S., Banerjee, S.K., 1976. On the possibility of obtaining relative paleointensities from lake sediments. Earth Planet. Sci. Lett. 29, 219–226.

Lhuillier, F., Fournier, A., Hulot, G., Aubert, J., 2011. The geomagnetic secular-variation timescale in observations and numerical dynamo models. Geophys. Res. Lett. 38, L09306, http://dx.doi.org/10.1029/2011GL047356.

Llave, E., Schonfeld, J., Hérnandez-Molina, F.J., Mulder, T., Somoza, L., Diaz del Rio, V., Sanchez-Almazo, I., 2006. High-resolution stratigraphy of the Mediterranean outflow contourite system in the Gulf of Cadiz during the late Pleistocene: The impact of Heinrich events. Mar. Geol. 227, 241–262.

Margari, V., Skinner, L.C., Tzedakis, P.C., Ganopolski, A., Vautravers, M., Shackleton, N.J., 2010. The nature of millennial-scale climate variability during the pas two glacial periods. Nat. Geosci. 3, 127–133.

Martrat, B., Grimalt, J.O., Shackleton, N.J., de Abrieu, L., Hutterli, M.A., Stocker, T.F., 2007. Four climate cycles of recurring deep and surface water destabilizations on the Iberian Margin. Science 317, 502–507.

Ménabréaz, L., Thouveny, N., Bourles, D.L., Deschamps, P., Hamelin, B., Demory, F., 2011. The Laschamp geomagnetic dipole low expressed as a cosmogenic ^{10}Be atmospheric overproduction at ∼41 ka. Earth Planet. Sci. Lett. 312, 305–317.

Mohamed, K.J., Rey, D., Rubio, B., Vilas, F., Frederichs, T., 2010. Interplay between detrital and diagenetic processes since the last glacial maximum on the northwest Iberian continental shelf. Quat. Res. 73, 507–520.

Moreno, E., Thouveny, N., Delanghe, D., McCave, I.N., Shackleton, N.J., 2002. Climatic and oceanographic changes in the Northeast Atlantic reflected by magnetic properties of sediments deposited on the Portuguese Margin during the last 340 ka. Earth Planet. Sci. Lett. 202, 465–480.

Muxworthy, A.R., Roberts, A.P., 2007. First-order reversal curve (FORC) diagrams. In: Gubbins, D., Herrero-Bervera, E. (Eds.), Encyclopedia of Geomagnetism and Paleomagnetism. Springer, Dordrecht, Netherlands, pp. 266–272.

Muxworthy, A.R., Williams, W., 2006. Critical single-domain/multidomain grain sizes in noninteracting and interacting elongate magnetite particles: Implications for magnetosomes. J. Geophys. Res. 111, B12S12, http://dx.doi.org/10.1029/2006JB004588.

Nicholl, J.A.L., Hodell, D.A., Naafs, B.D.A., Hillaire-Marcel, C., Channell, J.E.T., Romero, O.E., 2012. A Laurentide outburst flooding event during the last interglacial Period. Nat. Geosci., http://dx.doi.org/10.1038/NGEO1622.

Pike, C.R., Roberts, A.P., Verosub, K.L., 1999. Characterizing interactions in fine magnetic particle systems using first order reversal curves. J. Appl. Phys. 85, 6660–6667, http://dx.doi.org/10.1063/1.370176.

Roberts, A.P., Chiang, L., Heslop, D., Florindo, F., Larrasoana, J.C., 2012. Searching for single domain magnetite in the "pseudo-single-domain" sedimentary haystack: Implications of biogenic magnetite preservation for sediment magnetism and relative paleointensity determinations. J. Geophys. Res. 117, B08104, http://dx.doi.org/10.1029/2012JB009412.

Roberts, A.P., Florindo, F., Villa, G., Chang, L., Jovane, L., Bohaty, S.M., Larrasoana, J.C., Heslop, D., Fitz Gerald, J.D., 2011. Magnetotactic bacterial abundance in pelagic marine environments is limited by organic carbon flux and availability of dissolved iron. Earth Planet. Sci. Lett. 310, 441–452.

Roberts, A.P., Pike, C.R., Verosub, K.L., 2000. First-order reversal curve diagrams: A new tool for characterizing the magnetic properties of natural samples. J. Geophys. Res. 105, 28 461–28 475, http://dx.doi.org/10.1029/2000JB900326.

Robinson, S.G., 1986. The late Pleistocene palaeoclimatic record of north Atlantic deep-sea sediments revealed by mineral-magnetic measurements. Phys. Earth Planet. Inter. 42, 22–47.

Shackleton, N.J., Fairbanks, R.G., Chiu, T.-C., Parrenin, F., 2004. Absolute calibration of the Greenland time scale: Implications for Antarctic time scales and for Δ^{14}C. Quat. Sci. Rev. 23, 1513–1522.

Shackleton, N.J., Hall, M.A., Vincent, E., 2000. Phase relationships between millennial-scale events 64,000–24,000 years ago. Paleoceanography 15, 565–569.

Skinner, L.C., Elderfield, H., Hall, M., 2007. Phasing of millennial climate events and northeast Atlantic deep-water temperature change since 50 ka BP. In: Ocean Circulation: Mechanisms and Impacts. In: AGU Monogr., vol. 173, pp. 197–208.

Skinner, L.C., Shackleton, N.J., Elderfield, H., 2003. Millennial-scale variability of deep-water temperature and $\delta^{18}O_{dw}$ indicating deep-water source variations in the Northeast Atlantic, 0–34 cal. ka BP. Geochem. Geophys. Geosyst. 4, 1098, http://dx.doi.org/10.1029/2003GC000585.

Stow, D. Hernandez-Molina, F.J. Alvarez Zarikian, C.A. and Expedition 339 Scientists, 2012. Mediterranean outflow: Environmental significance of the Mediterranean Outflow Water and its global implications. IODP Preliminary Report, 339. http://dx.doi.org/10.2204/iodp.pr.339.2012.

Széréméta, N., Bassinot, F., Balut, Y., Labeyrie, L., Pagel, M., 2004. Oversampling of sedimentary series collected by giant piston corer: Evidence and corrections based on 3.5-kHz chirp profiles. Paleoceanography 19, PA1005, http://dx.doi.org/10.1029/2002PA000795.

Tauxe, L., 1993. Sedimentary records of relative paleointensity of the geomagnetic field: Theory and practice. Rev. Geophys. 31, 319–354.

Thomas, R., Guyodo, Y., Channell, J.E.T., 2003. U-channel track for susceptibility measurements. Geochem. Geophys. Geosyst. 1050, http://dx.doi.org/10.1029/2002GC000454.

Thomson, J., Nixon, S., Summerhayes, C.P., Rohling, E.J., Schonfeld, J., Zahn, R., Grootes, P., Abrantes, F., Gaspar, L., Vaqueiro, S., 2000. Enhanced productivity on the Iberian Margin during glacial/interglacial transitions revealed by barium and diatoms. J. Geol. Soc. 157, 667–677.

Thomson, J., Nixon, S., Summerhayes, C.P., Schonfeld, J., Zahn, R., Grootes, P., 1999. Implications for sedimentation changes on the Iberian Margin over the last two glacial/interglacial transitions from ($^{230}Th_{excess}$) systematics. Earth Planet. Sci. Lett. 165, 255–270.

Thouveny, N., Carcaillet, J., Moreno, E., Leduc, G., Nerini, D., 2004. Geomagnetic moment variation and paleomagnetic excursions since 400 kyr BP, a stacked record from sedimentary sequences of the Portuguese Margin. Earth Planet. Sci. Lett. 219, 377–396.

Thouveny, N., Moreno, E., Delanghe, D., Candon, L., Lancelot, Y., Shackleton, N.J., 2000. Rock-magnetic detection of distal ice rafted debris: Clue for the identification of Heinrich layers on the Portuguese Margin. Earth Planet. Sci. Lett. 180, 61–75.

Tzedakis, P.C., Palike, H., Roucoux, K.H., de Abreu, L., 2009. Atmospheric methane, Southern European vegetation and low mid-latitude links on orbital and millennial timescales. Earth Planet. Sci. Lett. 277, 307–317.

Tzedakis, P.C., Roucoux, K.H., de Abreu, L., Shackleton, N.J., 2004. The duration of forest stages in southern Europe and interglacial climate variability. Science 306, 2231–2235, http://dx.doi.org/10.1126/science.1102398.

Vali, H., Forster, O., Amarantidis, G., Petersen, N., 1987. Magnetotactic bacteria and their magnetofossils in sediments. Earth Planet. Sci. Lett. 86, 389–400.

Vautravers, M.J., Shackleton, N.J., 2006. Centennial-scale surface hydrology off Portugal during marine isotope stage 3: Insights from planktonic foraminiferal fauna variability. Paleoceanography 21, PA3004, http://dx.doi.org/10.1029/2005PA001144.

Voelker, A.H.L., de Abreu, L., 2011. A Review of Abrupt Climate Change Events in the Northeastern Atlantic Ocean (Iberian Margin): Latitudinal, Longitudinal and Vertical Gradients. In: Rashid, H., Polyak, L., Mosley-Thompson, E. (Eds.), Abrupt Climate Change: Mechanisms, Patterns, and Impacts. In: Geophys. Monogr., vol. 193. AGU, Washington DC, pp. 15–37. http://dx.doi.org/10.1029/2010GM001021.

Wang, H., Kent, D.V., Jackson, M.J., 2013. Evidence for abundant isolated magnetic nanoparticles at the Paleocene–Eocene boundary. Proc. Natl. Acad. Sci. USA 110 (2), 425–430.

Weeks, R., Laj, C., Endignoux, L., Fuller, M., Roberts, A., Manganne, R., Blanchard, E., Goree, W., 1993. Improvements in long-core measurement techniques: Applications in palaeomagnetism and palaeoceanography. Geophys. J. Int. 114, 651–662.

Westrich, J.T., Berner, R.A., 1984. The role of sedimentary organic matter in bacterial sulfate reduction: The G model tested. Limnol. Oceanogr. 29 (2), 236–249.

Xuan, C., Channell, J.E.T., 2009. UPmag: MATLAB software for viewing and processing u-channel or other pass-through paleomagnetic data. Geochem. Geophys. Geosyst. 10, Q10Y07, http://dx.doi.org/10.1029/2009GC002584.

Yamazaki, T., 2012. Paleoposition of the intertropical convergence zone in the eastern Pacific inferred from glacial-interglacial changes in terregenous and biogenic magnetic mineral fractions. Geology 40, 151–154.